nature structural & molecular biology

Energetic dissection of Gleevec's selectivity toward human tyrosine kinases

Roman V Agafonov[1,2], Christopher Wilson[1,2], Renee Otten[1], Vanessa Buosi[1] & Dorothee Kern[1]

Protein kinases are obvious drug targets against cancer, owing to their central role in cellular regulation. Since the discovery of Gleevec, a potent and specific inhibitor of Abl kinase, as a highly successful cancer therapeutic, the ability of this drug to distinguish between Abl and other tyrosine kinases such as Src has been intensely investigated but without much success. Using NMR and fast kinetics, we establish a new model that solves this longstanding question of how the two tyrosine kinases adopt almost identical structures when bound to Gleevec but have vastly different affinities. We show that, in contrast to all other proposed models, the origin of Abl's high affinity lies predominantly in a conformational change after binding. An energy landscape providing tight affinity via an induced fit and binding plasticity via a conformational-selection mechanism is likely to be general for many inhibitors.

The fundamental importance of protein kinases is indisputable. Their central role in essential physiological processes has provoked extensive studies and has resulted in a wealth of knowledge from biological signaling cascades to atomistic structural details[1–3]. Kinases are obvious attractive therapeutic drug targets because different signaling cascades can be selectively regulated by inhibiting individual kinases[4,5]. However, all kinases share a great degree of similarity, thus making it difficult to design inhibitors that are specific for a particular kinase[6–10]. This complication has hampered progress in drug development and highlights the need for a deeper understanding of the biophysical principles that govern kinase-drug interactions[11].

A prominent translational-research success story in treating chronic myeloid leukemia is the potent drug Gleevec (imatinib), which specifically targets the tyrosine kinase Abl. Its success is mainly due to the high specificity for the Abl subfamily of kinases as compared to its closest relative, the Src subfamily. The kinase domain of Src shares 54% sequence identity with Abl, and its drug-binding pocket with Gleevec bound is nearly identical to Abl's in both sequence and structure, but surprisingly Src has about 3,000 times weaker affinity for Gleevec[12]. The high clinical relevance and puzzling mismatch between structural similarity and different biochemical characteristics have placed the selectivity of Gleevec for Abl under intense scrutiny for the past 20 years but ultimately without decisive success[12].

Early crystal structures showed that the highly conserved Asp-Phe-Gly (DFG) motif, in the activation loop of kinases, adopts two distinct conformations in Src and Abl. It was therefore proposed that the inactive conformation of Src prevents Gleevec binding, owing to direct steric clashes[13–17]. However an important structure solved later revealed that Src is in fact capable of adopting the Abl-like clash-free inactive conformation[12]. Moreover, Abl was also found to be capable of adopting a Src-like inactive state[18]. With this initial hypothesis ruled out, two alternative explanations were put forward. According to the first one, the difference in affinity is due to subtle changes in the drug-binding pocket. Kuriyan and co-workers tested this idea by substituting residues in Src with the corresponding residues in Abl[12]. This extensive mutagenesis screening showed that none of the substitutions (alone or in combinations) resulted in substantial increase in Gleevec affinity. This led to an alternative hypothesis in which both enzymes are capable of adopting a DFG-out conformation, but they differ in the probability of occupying that conformation; thus, binding of Gleevec is regulated via a conformational-selection mechanism[12,19–23]. Monitoring the dynamics of the DFG loop in kinases by NMR[24,25] has not been successful because the corresponding peaks were missing in the apo spectra. Owing to the lack of experimental results, several groups used molecular dynamics simulations to calculate different components of the free energy of Gleevec binding, rationalizing the huge difference in affinity with controversial conclusions[19–21,26]. In summary, the question of why Gleevec is a potent inhibitor of Abl but not Src remains controversial and unresolved[20]. Here we set out to address this open energetic question.

The extensive history of protein biochemistry has shown that kinetic and energetic properties can rarely be inferred from high-resolution crystal structures alone. In this work, we use a combination of pre-steady-state fluorescence kinetics and NMR spectroscopy to study directly the process of Gleevec binding to the catalytic domain of Abl and Src with millisecond time resolution and residue-specific precision. These data reveal a new mechanism for Gleevec binding that quantitatively accounts for the difference in Gleevec affinity between Src and Abl.

RESULTS

NMR titration of Gleevec reveals an induced-fit mechanism

Binding of an inhibitor to its target protein is a dynamic process that cannot be understood solely on the basis of structural data. NMR can

[1]Howard Hughes Medical Institute, Department of Biochemistry, Brandeis University, Waltham, Massachusetts, USA. [2]These authors contributed equally to this work. Correspondence should be addressed to D.K. (dkern@brandeis.edu).

Received 15 July; accepted 20 August; published online 14 September 2014; doi:10.1038/nsmb.2891

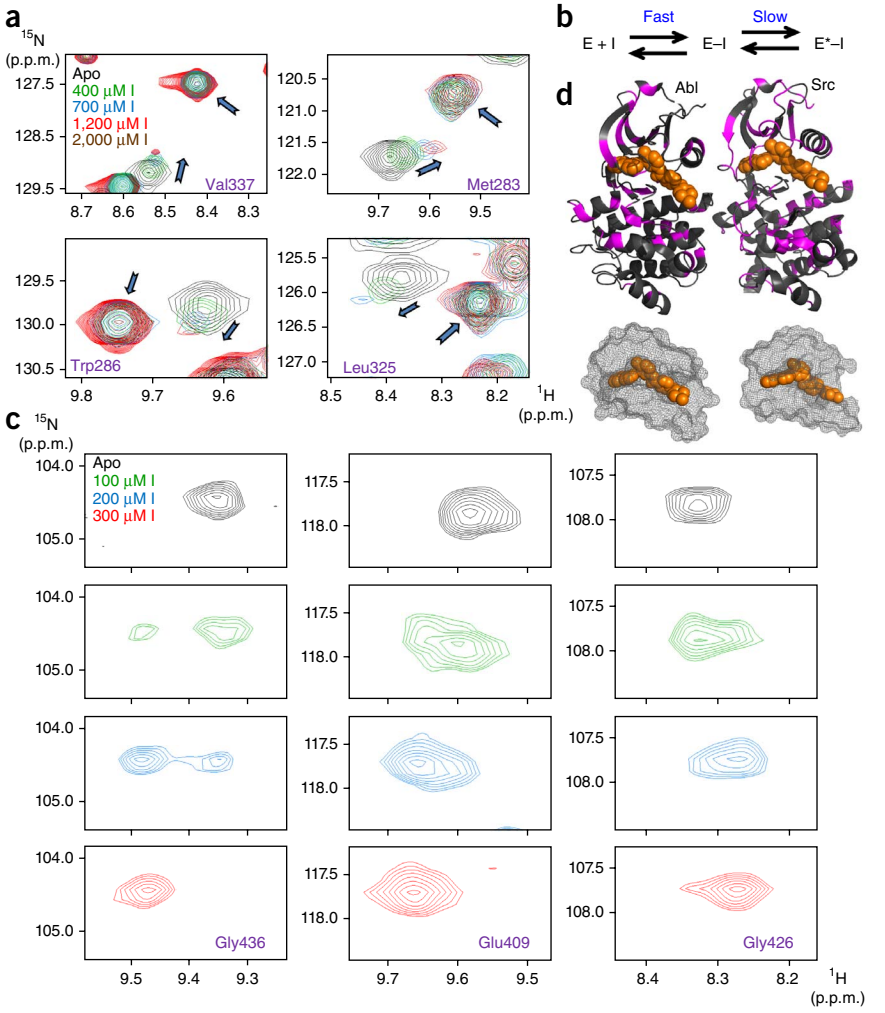

Figure 1 Monitoring the process of Gleevec binding to Src and Abl by NMR at 25 °C. (**a**) Zoom of ^{1}H-^{15}N–HSQC spectra showing an unusual pattern of chemical-shift perturbations (shifting of free peak position coinciding with the reappearance of the Gleevec-bound peak) upon titration of Src (250 μM) with Gleevec. (**b**) Biochemical scheme that can explain the observed titration patterns[27] (additional data in **Supplementary Fig. 1**). E and E–I correspond to free and inhibitor-bound kinase; E*–I corresponds to inhibitor-bound kinase in a distinct conformational state. (**c**) 250 μM Abl titration showing a simpler pattern with disappearance and reappearance of the peaks indicative of tight binding. (**d**) Residues with chemical-shift changes upon Gleevec binding plotted onto the crystal structures of Abl and Src (PDB 1OPJ[31] and 2OIQ[12], respectively) in magenta, with Gleevec shown in orange. The mesh representation of the Gleevec-binding pocket illustrates how part of the drug is covered by the protein and suggests a conformational change after binding (second step in **Fig. 1b**).

provide information about structural changes within a protein during binding and detect timescales of these processes. To this end, we titrated Gleevec into Src and Abl and used ^{1}H-^{15}N–HSQC spectra to monitor the binding (**Fig. 1**). In the case of Src, the pattern of peak movement was unusual. Upon addition of increasing amounts of drug, peaks gradually shifted and simultaneously appeared at new positions (**Fig. 1a**). In general, peak shifting in a titration experiment indicates that the corresponding residue is in fast exchange between two states (>100 s^{-1} for typical chemical-shift differences). This is in contrast to slow exchange (<1 s^{-1}), wherein peaks disappear at one position and appear at another. In our case, we observed both phenomena simultaneously, indicating that Gleevec binding is at least a two-step process, with one of the steps being fast and the other one slow. Residues that showed chemical-shift perturbations upon addition of Gleevec were not clustered around the Gleevec-binding site or the DFG loop. Instead they were distributed over a large fraction of the protein, suggesting a global conformational change (**Fig. 1d**). In general, such a conformational change can happen before or after binding. To differentiate between these two scenarios, we simulated the spectroscopic behavior for all possible binding models[27] (**Supplementary Fig. 1a–d**). The only scheme compatible with the observed pattern (**Fig. 1a**) is the one in which Gleevec binding is fast and is followed by a slow conformational change (**Fig. 1b**).

This model of Gleevec binding is dramatically different from the models proposed earlier in two distinct ways. First, our data uncover a previously undescribed step: a structural transition that follows Gleevec binding (E–I ↔ E*–I, in which E–I and E*–I represent the two distinct conformations of the kinase (E, enzyme) with Gleevec bound (I, inhibitor)) and stabilizes the Src–Gleevec complex. Second, in contrast to previous observations, this scheme implies that Gleevec binding is fast, and the rate-limiting step is, in fact, the structural transition.

NMR titration of Abl with Gleevec showed a simpler pattern (**Fig. 1c**) with peaks disappearing at one position and appearing at a second position. This is an indication that in Abl the E–I ↔ E*–I equilibrium is shifted far toward the E*–I state (**Fig. 1b**), thus resulting in a negligible population of the E–I complex at any concentration of the drug. In such a scenario, the fast drug-binding step is undetectable (**Supplementary Fig. 1e**). This NMR spectroscopic pattern could also naturally be explained by a simple two-state mechanism (E + I ↔ E–I, in which E, I and E–I are apo kinase, Gleevec and kinase–Gleevec complex, respectively); however, such a model was ruled out by experiments described below. Such fundamentally distinct spectroscopic characteristics delivered the first sign that the difference in enzyme affinities is not due to the difference in the initial binding step but is instead caused by a different conformational equilibrium after binding.

Real-time Gleevec binding kinetics

To buttress this hypothesis and to quantitatively characterize the energetics of Gleevec binding to Src and Abl, we performed a series of rapid-mixing experiments that allowed direct monitoring of inhibitor binding kinetics. We detected complex formation and conformational changes by using the enzymes' intrinsic tryptophan fluorescence. For inhibitor binding to either enzyme, fluorescence kinetics at all Gleevec concentrations could be adequately fit by a single exponential at 25 °C (**Fig. 2a,b**). Interestingly, the dependence of the observed rate on drug concentration is nonlinear, with an apparent plateau at approximately 20 s^{-1} and 2 s^{-1} for Abl and Src, respectively (**Fig. 2c,d**).

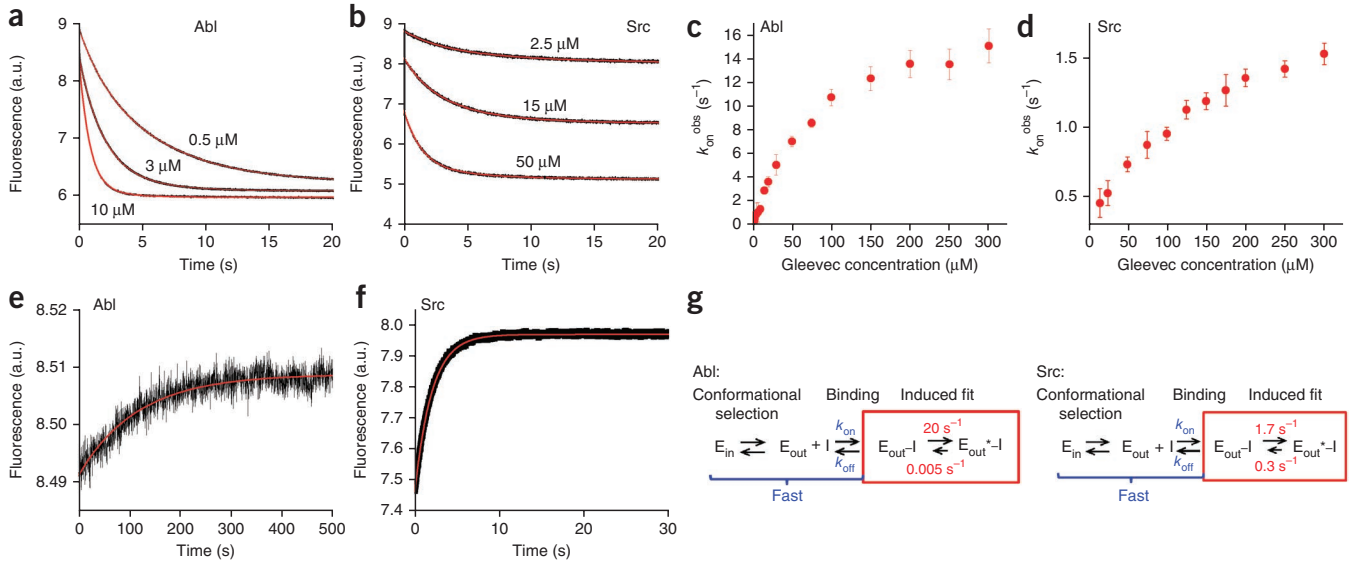

Figure 2 Kinetics of Gleevec binding to Abl and Src at 25 °C. (**a**,**b**) Tryptophan fluorescence change after mixing Abl (**a**) or Src (**b**) with increasing amounts of Gleevec. Kinetics of both Abl and Src are monoexponential. (**c**,**d**) Observed rates (k_{on}^{obs}) for Gleevec binding to Abl (**c**) and Src (**d**), which do not show the expected linear dependence on the Gleevec concentration but exhibit a curvature approaching a plateau, in agreement with the proposed binding scheme in **Figure 1b** ($n = 3$ experiments; mean ± s.e.m.). (**e**,**f**) Dissociation kinetics of Gleevec from Abl (**e**) and Src (**f**), measured by dilution of Abl–Gleevec and Src–Gleevec complexes, respectively. (**g**) Binding scheme highlighting a 1,000-fold-tighter affinity for Abl caused by a newly identified conformational step after binding (red). E_{in} and E_{out} define apo kinase with the DFG loop in the in and out positions, respectively. E_{out}–I and E_{out}*–I are the respective Gleevec-bound complexes. The relevant rate constants are defined.

How could these data be interpreted? Nonlinear concentration dependence of the observed binding rates indicates that it is not a simple pseudo-first-order binding but rather that protein conformational transitions are rate limiting, in agreement with the scheme in **Figure 1b**. At the same time, this scheme implies a two-step process that should be characterized by double-exponential kinetics, which is not observed. To resolve this apparent contradiction, we repeated the experiments at 5 °C with the idea to slow down processes that might have been unresolved previously. At this temperature, Gleevec binding to Abl is indeed clearly double exponential (**Fig. 3a**). The fast phase ($k^{obs}{}_{bind}$) follows a linear dependence on Gleevec concentration (**Fig. 3e**) corresponding to the binding step, whereas the slower step ($k^{obs}{}_{conf}$) shows the curvature (**Fig. 3f**) seen before in **Figure 2c** and corresponds to the conformational transition after binding (induced fit) (**Fig. 2g** and **Table 1**). Fits of these data demonstrate that rate constants for the binding step are fast, with $k_{on} = 1.5\ \mu M^{-1}\ s^{-1}$ and $k_{off} = 25\ s^{-1}$, respectively, and that the conformational transition is substantially slower (Online Methods) This implies that the rates determined at 25 °C reflect the conformational transitions and that the faster phase is not observed because at the higher temperature binding is finished within the dead time of the instrument (5 ms). With this insight, **Figure 2a–d** has the following interpretation:

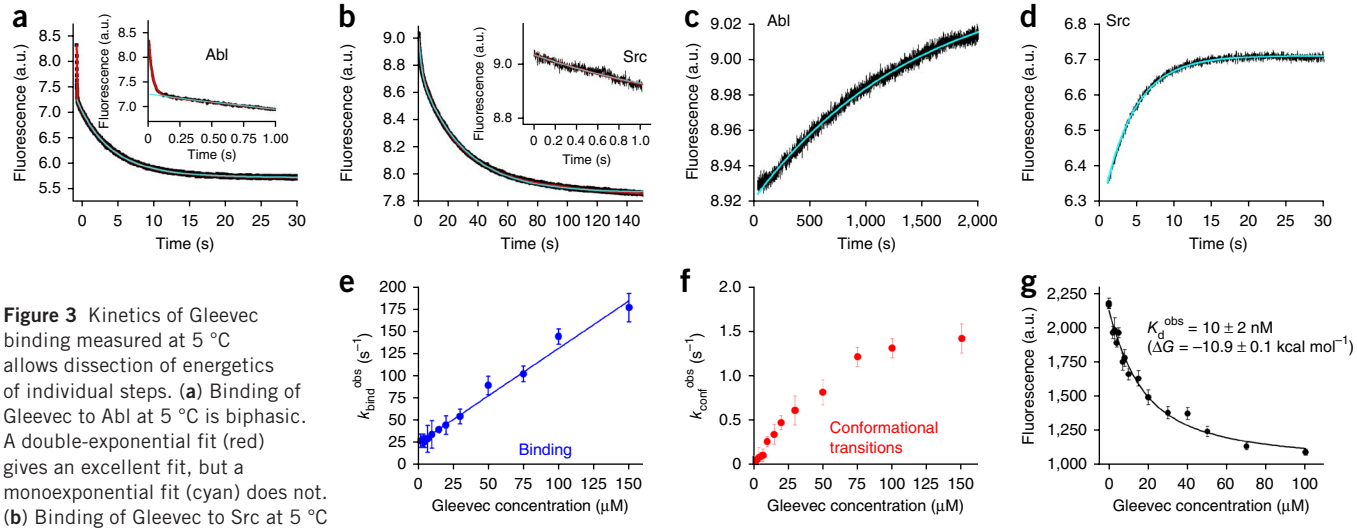

Figure 3 Kinetics of Gleevec binding measured at 5 °C allows dissection of energetics of individual steps. (**a**) Binding of Gleevec to Abl at 5 °C is biphasic. A double-exponential fit (red) gives an excellent fit, but a monoexponential fit (cyan) does not. (**b**) Binding of Gleevec to Src at 5 °C is monophasic. A monoexponential fit (cyan) is as good as a double-exponential fit (red). Insets in (**a**) and (**b**) show a zoomed-in view of the first second of the kinetics. (**c**,**d**) Dissociation of Gleevec from Abl (**c**) and Src (**d**). (**e**,**f**) Concentration dependence of the fast (**e**) and slow (**f**) phases of Gleevec binding to Abl, identifying them as the binding and conformational step, respectively ($n = 3$ experiments; mean ±s.e.m.). (**g**) Gleevec's overall observed K_d^{obs} to Abl at 5 °C, determined independently via steady-state measurement of tryptophan fluorescence quenching by Gleevec ($n = 3$ experiments; mean ±s.e.m.).

Table 1 Rate constants of binding (k_{on} and k_{off}) and conformational-change steps (k_{conf+} and k_{conf-}) and corresponding K_d and ΔG in the Abl-Gleevec binding scheme

Binding	Conformational change
$k_{off} = 25 \pm 6\ s^{-1}$ $k_{on} = 1.5 \pm 0.1\ \mu M^{-1}\ s^{-1}$	$k_{conf-} = (7 \pm 1) \times 10^{-4}\ s^{-1}$ $k_{conf+} = 1.5 \pm 0.2\ s^{-1}$
$K_d^{bind} = 17 \pm 4\ \mu M$ ($\Delta G = -6.5 \pm 0.1$ kcal mol^{-1})	$K_d^{conf} = (4.7 \pm 0.9) \times 10^{-4}$ ($\Delta G = -4.5 \pm 0.1$ kcal mol^{-1})
$K_d^{kin} = K_d^{bind} \times K_d^{conf} / (1 + K_d^{conf}) = 8 \pm 3$ nM ($\Delta G = -11 \pm 0.3$ kcal mol^{-1})	

Data from **Figure 3**.

binding of the drug to both enzymes is fast, and the observed kinetics reflects the conformational transition induced by Gleevec. The fact that the observed rate of a conformational transition depends on ligand concentration might be counterintuitive, but at increasing drug concentration the transient concentration of the E–I complex increases, and this leads to an increase of the apparent rate (**Figs. 1b** and **2c**,**d** and Online Methods). We note that the binding step was not directly observable for Src, owing to a too-small population of the binding-competent state, as discussed below (**Supplementary Fig. 2**).

Determining factor for dramatic difference in Gleevec's affinity

Where do these kinetic experiments take us in understanding the underlying mechanism for the 3,000-fold difference in Gleevec affinity? A final experiment, measuring the kinetics of dissociation, completes the puzzle. To initiate dissociation, we rapidly diluted enzyme incubated with Gleevec by 11-fold. The observed rate of fluorescence change was remarkably slow, especially in Abl (**Figs. 2e**,**f** and **3c**). Considering that even at 5 °C the actual 'off' rate constant from the E–I state was 25 s^{-1} (**Fig. 3e** and **Table 1**), the observed slow process must be attributed to slow conformational change from E*–I to E–I. Thus we can conclude that the rate constants 0.3 s^{-1} and 0.005 s^{-1} obtained in the dilution experiments correspond to the E*–I → E–I transition in Src and Abl, respectively (**Fig. 2g**).

Strikingly, the measured difference in the conformational equilibrium between two drug-bound states accounts for an approximately 1,000-fold difference in Gleevec affinity between Abl and Src: the forward rate constants differ ten-fold, and the difference in the reverse direction is about another two orders of magnitude (**Fig. 2g**). These two effects account for all but three-fold of the overall Gleevec binding affinity. This remaining difference probably arises from differences in the E_{in}/E_{out} equilibrium in the apo protein (corresponding to the in and out positions of the DFG loop) and/or the binding step (**Fig. 2g**).

Energetic dissection of individual binding steps

The fact that both phases can be observed for Abl at 5 °C enabled us to calculate the K_d for Gleevec binding purely on the basis of the measured kinetics (K_d^{kin}) and then to compare it with the global K_d^{obs} from thermodynamic experiments (**Fig. 3g**). These two independently determined K_d values are remarkably close (**Table 1** and **Fig. 3g**), substantiating our new proposed mechanism underlying Gleevec specificity. As a second test of our model, we performed a global fit of all fluorescence kinetics data, using numerical simulations (**Fig. 4**)[28]. First, all fitted microscopic rate constants are in excellent agreement with the values from the analysis described in **Figure 3**, and, second, possible alternative models fail to fit the data (**Supplementary Figs. 3** and **4**).

Importantly, the kinetic experiments deliver a quantitative dissection of the binding free-energy contributions from each microscopic step, highlighting that almost half of the favorable free energy comes from the conformational transition after binding (**Table 1**). It is exactly this step that accounts for Abl's ability to tightly bind

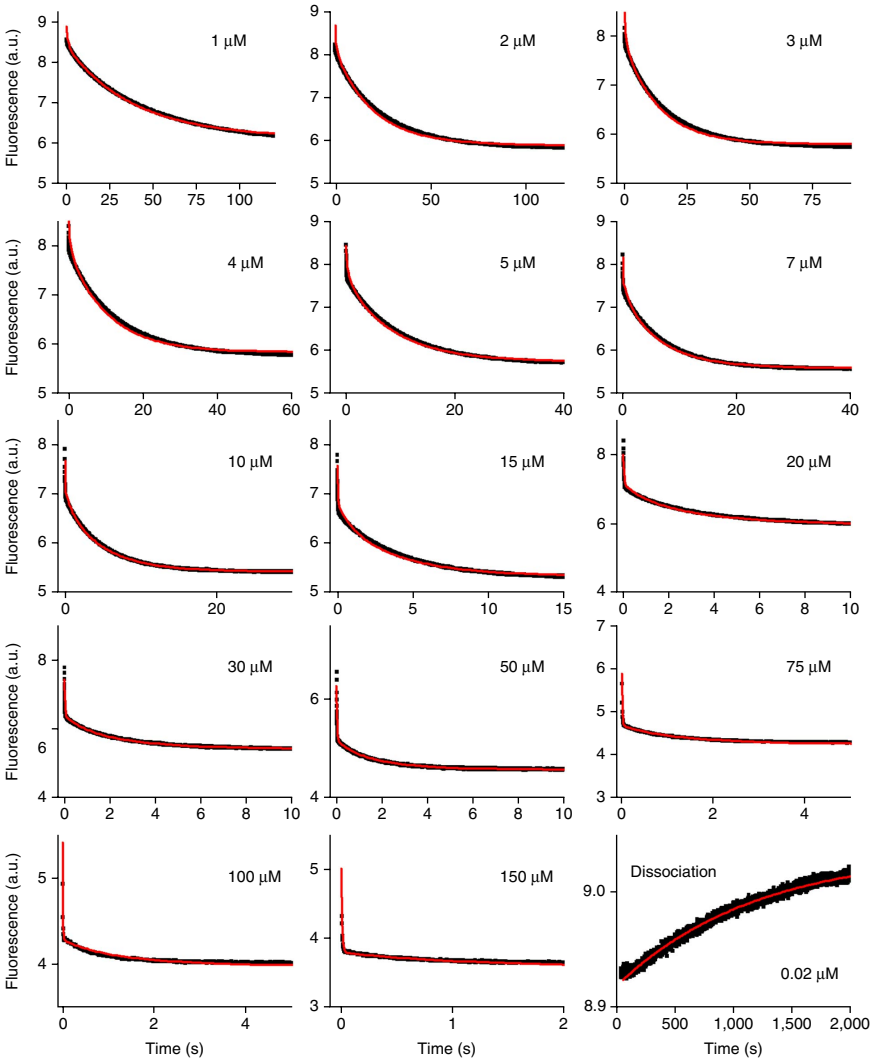

Figure 4 Global fit of Gleevec binding and dissociation kinetics to Abl measured by tryptophan fluorescence at 5 °C. Black circles, experimental data; red lines, global numerical simulation of the whole data set with Kintek Explorer[28,32]. The induced-fit model (E ↔ E–I ↔ E*–I) was used, and the global fitting results ($k_{on} = 1.3 \pm 0.3\ \mu M^{-1} s^{-1}$, $k_{off} = 23 \pm 5\ s^{-1}$, $k_{conf+} = 1.3 \pm 0.2\ s^{-1}$ and $k_{conf-} = (6 \pm 2) \times 10^{-4}\ s^{-1}$) were in excellent agreement with individual fits (**Table 1**), validating the robustness of the model.

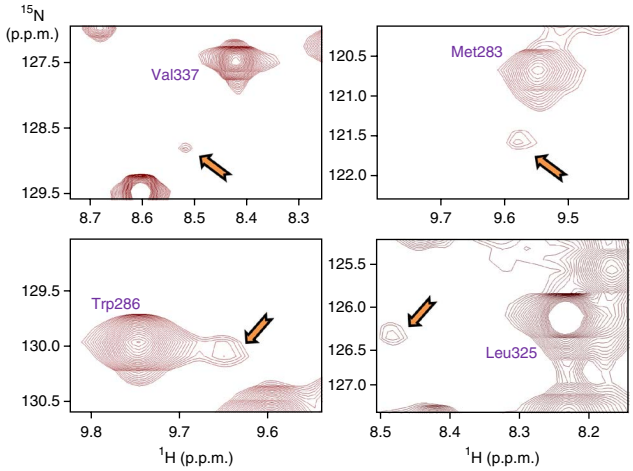

Figure 5 Direct observation of the conformational-exchange step in the Src–Gleevec complex by NMR. ^{1}H-^{15}N–HSQC spectrum of Src at saturating Gleevec concentrations recorded for 16 h, showing the presence of major and minor peaks corresponding to the Src*–I and Src–I complexes, respectively. The minor peaks appear exactly where predicted from the Gleevec titrations (**Fig. 1a** and **Supplementary Fig. 5**).

Gleevec in contrast to Src, with a difference of –4.6 kcal mol^{-1} between them, leaving only a minor energy contribution from the widely proposed DFG_{in}-DFG_{out} flip[12,19–21].

Direct detection of the higher-energy E–I state in Src

Because our mechanism differs drastically from the current paradigm in the field[12,19–21], we felt the need to design an additional experiment that could directly detect this critical conformational transition of the kinase–Gleevec complex. Close examination of the rate constants in the scheme (**Fig. 2g**) showed that in Src, the E–I ↔ E*–I equilibrium is slow on the NMR timescale and is only moderately skewed (~15% in the E–I state), thus suggesting that peaks corresponding to this state should be directly visible in the HSQC spectrum of Src saturated with Gleevec. Because we did not observe this in our original titration (**Fig. 1a**), and such a spectroscopic feature was not seen in previous NMR data published on the Src–Gleevec complex[29], we recorded spectra for 16 h to increase the signal-to-noise ratio. This maneuver indeed revealed the presence of minor peaks at positions corresponding to the E–I state (**Fig. 5** and **Supplementary Fig. 5**) with relative populations of the E–I and E*–I states being in agreement with the kinetics data (**Fig. 2g**). The same experiment performed on the Abl–Gleevec complex showed no minor peaks, in agreement with our conclusion that for Abl, the E–I ↔ E*–I equilibrium lies far toward the Abl*–I state (**Fig. 2g**). Our data establish a new model that resolves the controversy of how Src and Abl have drastically different affinities for the clinically relevant drug Gleevec despite adopting almost identical structures when bound to it. The relatively large number of residues sensing conformational changes induced by Gleevec binding is in agreement with suggestions by Kuriyan and co-workers based on mutagenesis efforts[12] and a recent NMR study of full-length Abl[30].

DISCUSSION

These results enable us to envision the free-energy landscape of Gleevec binding and provide a quantitative rationale for Gleevec selectivity. Multiple lines of evidence, including direct detection of Gleevec binding by NMR and stopped-flow fluorescence, identify an induced-fit conformational change in the kinase–Gleevec complex as the origin of the observed high affinity of Gleevec for Abl. For Gleevec, the physical binding step results in only micromolar affinities for both Abl and Src, and only the induced-fit step brings Abl's affinity into the clinically relevant nanomolar range. However, the ability of Abl and Src to sample the binding-competent DFG-out state (E_{out}) enables binding of Gleevec. Such sampling of multiple conformations by the apo enzyme (i.e., conformational selection) by definition weakens affinity by the fraction of the enzyme in the binding-incompetent state, but is required for more-selective drugs that bind only to a unique enzyme conformation. This is in contrast to nonselective drugs that easily bind to multiple conformations and hence multiple targets[1,11,21]. The effect of increasing and decreasing affinities via induced fit versus conformational selection (E_{out}–I ↔ E_{out}*–I and E_{in} ↔ E_{out} steps in the case of Abl and Src) is, of course, based on simple thermodynamics of coupled equilibria. The free-energy landscape of Gleevec binding to two important drug targets, characterized here, illustrates how nature has solved the dual challenge of having high selectivity while maintaining strong affinity. Such principles may be general for many other tight-binding inhibitors. Although the detailed path to rational drug design, encompassing the points above, is long, the first steps are to characterize a quantitative model for binding, as performed here, and then to identify the key residues underlying the energetics of binding (C.W., R.V.A. and D.K., unpublished data). Computation undoubtedly has a key role in the energy calculations and design part, but using the correct binding model with quantitative experimental data is crucial, as best illustrated by the history of understanding Gleevec selectivity by computation[19–21]. By analogy with the advances in predicting protein structures, using the large set of structural data combined with energy functions, we anticipate that availability of extensive quantitative data on the detailed energetics of drug binding as delivered here may have a big impact on rational drug design.

METHODS

Methods and any associated references are available in the online version of the paper.

Note: Any Supplementary Information and Source Data files are available in the online version of the paper.

ACKNOWLEDGMENTS

We are grateful to M.A. Morando and F. Gervasio (Spanish National Cancer Research Center) for providing plasmids for the Src kinase domain and for sharing expression and purification protocols. This work was supported by the Howard Hughes Medical Institute (HHMI), the Office of Basic Energy Sciences, Catalysis Science Program, US Department of Energy, award DE-FG02-05ER15699 and the US National Institutes of Health GM100966 to D.K. R.O. is supported as an HHMI Fellow of the Damon Runyon Cancer Research Foundation, DRG-2114-12.

AUTHOR CONTRIBUTIONS

R.V.A. and C.W. contributed equally to this work. R.V.A., C.W. and D.K. designed and analyzed all experiments; R.V.A. and C.W. performed experiments; R.O. assisted with NMR data acquisition and analysis; V.B. assisted with MS experiments; and R.V.A, C.W. and D.K. wrote the manuscript with contributions from all authors.

COMPETING FINANCIAL INTERESTS

The authors declare no competing financial interests.

1. Jura, N. *et al.* Catalytic control in the EGF receptor and its connection to general kinase regulatory mechanisms. *Mol. Cell* **42**, 9–22 (2011).
2. Kornev, A.P. & Taylor, S.S. Defining the conserved internal architecture of a protein kinase. *Biochim. Biophys. Acta* **1804**, 440–444 (2010).

3. Taylor, S.S., Keshwani, M.M., Steichen, J.M. & Kornev, A.P. Evolution of the eukaryotic protein kinases as dynamic molecular switches. *Phil. Trans. R. Soc. Lond. B* **367**, 2517–2528 (2012).
4. Hunter, T. Tyrosine phosphorylation: thirty years and counting. *Curr. Opin. Cell Biol.* **21**, 140–146 (2009).
5. Cohen, P. Protein kinases: the major drug targets of the twenty-first century? *Nat. Rev. Drug Discov.* **1**, 309–315 (2002).
6. Huse, M. & Kuriyan, J. The conformational plasticity of protein kinases. *Cell* **109**, 275–282 (2002).
7. Nagar, B. c-Abl tyrosine kinase and inhibition by the cancer drug imatinib (Gleevec/STI-571). *J. Nutr.* **137**, 1518S–1523S (2007).
8. Harrison, S.C. Variation on an Src-like theme. *Cell* **112**, 737–740 (2003).
9. Azam, M. *et al.* Activity of dual SRC-ABL inhibitors highlights the role of BCR/ABL kinase dynamics in drug resistance. *Proc. Natl. Acad. Sci. USA* **103**, 9244–9249 (2006).
10. Winter, G.E. *et al.* Systems-pharmacology dissection of a drug synergy in imatinib-resistant CML. *Nat. Chem. Biol.* **8**, 905–912 (2012).
11. Dar, A.C. & Shokat, K.M. The evolution of protein kinase inhibitors from antagonists to agonists of cellular signaling. *Annu. Rev. Biochem.* **80**, 769–795 (2011).
12. Seeliger, M.A. *et al.* c-Src binds to the cancer drug imatinib with an inactive Abl/c-Kit conformation and a distributed thermodynamic penalty. *Structure* **15**, 299–311 (2007).
13. Nagar, B. *et al.* Crystal structures of the kinase domain of c-Abl in complex with the small molecule inhibitors PD173955 and imatinib (STI-571). *Cancer Res.* **62**, 4236–4243 (2002).
14. Schindler, T. *et al.* Structural mechanism for STI-571 inhibition of abelson tyrosine kinase. *Science* **289**, 1938–1942 (2000).
15. Williams, J.C. *et al.* The 2.35 A crystal structure of the inactivated form of chicken Src: a dynamic molecule with multiple regulatory interactions. *J. Mol. Biol.* **274**, 757–775 (1997).
16. Xu, W., Doshi, A., Lei, M., Eck, M.J. & Harrison, S.C. Crystal structures of c-Src reveal features of its autoinhibitory mechanism. *Mol. Cell* **3**, 629–638 (1999).
17. Xu, W., Harrison, S.C. & Eck, M.J. Three-dimensional structure of the tyrosine kinase c-Src. *Nature* **385**, 595–602 (1997).
18. Levinson, N.M. *et al.* A Src-like inactive conformation in the abl tyrosine kinase domain. *PLoS Biol.* **4**, e144 (2006).
19. Aleksandrov, A. & Simonson, T. Molecular dynamics simulations show that conformational selection governs the binding preferences of imatinib for several tyrosine kinases. *J. Biol. Chem.* **285**, 13807–13815 (2010).
20. Lin, Y.L., Meng, Y., Jiang, W. & Roux, B. Explaining why Gleevec is a specific and potent inhibitor of Abl kinase. *Proc. Natl. Acad. Sci. USA* **110**, 1664–1669 (2013).
21. Lovera, S. *et al.* The different flexibility of c-Src and c-Abl kinases regulates the accessibility of a druggable inactive conformation. *J. Am. Chem. Soc.* **134**, 2496–2499 (2012).
22. Cowan-Jacob, S.W. *et al.* The crystal structure of a c-Src complex in an active conformation suggests possible steps in c-Src activation. *Structure* **13**, 861–871 (2005).
23. Dar, A.C., Lopez, M.S. & Shokat, K.M. Small molecule recognition of c-Src via the Imatinib-binding conformation. *Chem. Biol.* **15**, 1015–1022 (2008).
24. Vajpai, N. *et al.* Solution conformations and dynamics of ABL kinase-inhibitor complexes determined by NMR substantiate the different binding modes of imatinib/nilotinib and dasatinib. *J. Biol. Chem.* **283**, 18292–18302 (2008).
25. Vogtherr, M. *et al.* NMR characterization of kinase p38 dynamics in free and ligand-bound forms. *Angew. Chem. Int. Edn. Engl.* **45**, 993–997 (2006).
26. Shan, Y. *et al.* A conserved protonation-dependent switch controls drug binding in the Abl kinase. *Proc. Natl. Acad. Sci. USA* **106**, 139–144 (2009).
27. Kovrigin, E.L. NMR line shapes and multi-state binding equilibria. *J. Biomol. NMR* **53**, 257–270 (2012).
28. Johnson, K.A. Fitting enzyme kinetic data with KinTek Global Kinetic Explorer. *Methods Enzymol.* **467**, 601–626 (2009).
29. Campos-Olivas, R., Marenchino, M., Scapozza, L. & Gervasio, F.L. Backbone assignment of the tyrosine kinase Src catalytic domain in complex with imatinib. *Biomol. NMR Assign.* **5**, 221–224 (2011).
30. Skora, L., Mestan, J., Fabbro, D., Jahnke, W. & Grzesiek, S. NMR reveals the allosteric opening and closing of Abelson tyrosine kinase by ATP-site and myristoyl pocket inhibitors. *Proc. Natl. Acad. Sci. USA* **110**, E4437–E4445 (2013).
31. Nagar, B. *et al.* Structural basis for the autoinhibition of c-Abl tyrosine kinase. *Cell* **112**, 859–871 (2003).
32. Johnson, K.A., Simpson, Z.B. & Blom, T. FitSpace explorer: an algorithm to evaluate multidimensional parameter space in fitting kinetic data. *Anal. Biochem.* **387**, 30–41 (2009).

ONLINE METHODS

Protein expression and purification. Genes corresponding to kinase domains of Abl and Src were subcloned into an expression vector containing histidine (for Src) or histidine/MBP (for Abl) tags for growth in the BL21 (DE3) cell line. Cells were cotransformed with the YOPH phosphatase to ensure a dephosphorylated state of expressed protein and to lower toxicity due to overexpression. Culture was grown to OD of 0.8 at 37 °C and then switched to 20 °C and induced with 200 μM of IPTG overnight. Protein was purified with a combination of ion-affinity, anion-exchange, and size-exclusion columns. Affinity tags were removed by overnight incubation with TEV protease. Purity of the protein was confirmed by gel electrophoresis, and lack of tyrosine phosphorylation was confirmed by MS. For NMR experiments, U-^{15}N– and U-^{2}H, ^{15}N–labeled proteins were expressed in M9 minimal medium prepared with H_2O or D_2O, respectively. In both cases, the M9 medium contained 1 g/L $[^{15}N]H_4Cl$ as the sole nitrogen source and 3 g/L unlabeled D-glucose.

NMR experiments. ^{1}H-^{15}N–TROSY-HSQC experiments were performed at 25 °C on an Agilent DD2 600 MHz four-channel spectrometer equipped with a triple-resonance cryogenically cooled probe head. To increase stability of the samples, buffer compositions were optimized with a thermofluor-based high-throughput stability assay[33]. Solutions of Sypro Orange were mixed with 5 μL of protein at 100 μM and 15 μL of buffer of interest and added to a 96-well PCR plate. A control sample contained buffer and Sypro Orange only. The plates were sealed with optical sealing tape and heated in a real-time PCR machine from 20 to 100 °C with increments of 0.2 °C. Fluorescence was measured by exciting at 490 nm and measuring at 575 nm. Optimized NMR samples contained 250–500 μM protein and 10% (v/v) D_2O in either 50 mM Tris, 500 mM NaCl, 1 mM $MgCl_2$ and 1 mM TCEP, pH 8.0, or 10 mM EPPS, 100 mM NaCl and 1 mM TCEP, pH 8.0. NMR data were processed with NMRPipe/NMRDraw[34] and analyzed with CcpNmr[35].

Pre-steady-state kinetics experiments. Stopped-flow experiments were performed with the Applied Photophysics SX-20 instrument equipped with a temperature-control unit. Gleevec binding kinetics was monitored via changes in intrinsic tryptophan fluorescence. Samples were excited at 295 nm (9 nm bandwidth), and emission was detected with a long-pass 320 nm–cutoff filter. To overcome Gleevec solubility issues, a nonequal mixing ratio was used. Protein was loaded into a 0.5-mL syringe, and the drug was loaded into a 5-mL syringe, resulting in a 1-to-10 mixing-volume ratio. The final protein concentration was typically 0.1 μM, and Gleevec concentration was varied. To study dissociation kinetics, protein (at 0.1–1 μM) was preincubated with 0.1–100 μM of Gleevec for 10 min, placed into the 0.5-mL syringe and then diluted with buffer loaded into the 5-mL syringe. This setup allowed for an 11-fold dilution. All experiments were performed at 5 °C and 25 °C in a buffer containing 50 mM Tris, 500 mM NaCl, 1 mM $MgCl_2$, 1 mM TCEP and 5% DMSO, pH 8.0.

Data were analyzed with Applied Photophysics or Origin (OriginLab Corporation) software. Individual fluorescent transients were fitted to single- or multiexponential curves. To account for photobleaching, an additional exponential term was added to the fitting function. This rate was fixed to the value determined in control experiments in which protein was mixed with buffer in the absence of Gleevec.

Association and dissociation of Gleevec with Abl at 5 °C (when both binding and conformational transitions could be clearly resolved) were also simulated and fitted globally with numerical algorithms with KinTek explorer[28,32]. In these simulations, the same set of kinetic rate constants was used to fit all 15 data sets corresponding to different Gleevec concentrations.

Measurements of Gleevec affinity. Gleevec affinity to Abl at 5 °C was measured with a Hitachi F-2500 fluorimeter. 10 nM of Abl was mixed with 2 nM to 75 nM of Gleevec. Binding was monitored via changes in tryptophan fluorescence. Tryptophans were excited at 295 nm, and fluorescence was detected at 350 nm. Extracted intensities were fit to a generalized binding equation

$$F = F_0 + A \times \frac{[\mathrm{I}] + [\mathrm{E_t}] + K_\mathrm{d} - \sqrt{([\mathrm{I}] + [\mathrm{E_t}] + K_\mathrm{d})^2 - 4 \times [\mathrm{E_t}] \times [\mathrm{I}]}}{2 \times [\mathrm{E_t}]}$$

where $[E_t]$ is total enzyme concentration, [I] is the concentration of Gleevec, and F_0 and A are background fluorescence and a scaling factor, respectively.

Analysis of kinetic data. The following naming conventions are used throughout the text: (i) Different states of enzyme without or with bound inhibitor are called E, E–I and E*–I. (ii) In cases in which conformation of the DFG loop is specified, subscripts 'in' or 'out' are added (for example, E_{in}, E_{out}, E_{out}–I, etc.). (iii) Rates describing the time dependence of experimentally observed changes in fluorescence are called observed rates or apparent rates. (iv) k_{on}, k_{off}, k_{conf+} and k_{conf-} are called rate constants and correspond to individual microscopic steps in the reaction schemes. They are specified in **Figure 2g**. (v) F denotes the amplitude of the observed fluorescence signal and is generated by combined fluorescence from all enzyme species.

In the case of a simple pseudo-first-order reaction (a two-state model), the time dependence of the fluorescence signal is monoexponential (**Supplementary Fig. 6a**). Binding and dissociation (k_{on} and k_{off}, respectively) rate constants can be determined from the plot of the observed rate as a function of inhibitor concentration (**Supplementary Fig. 6b**), in which the slope is equal to k_{on}, and the intercept corresponds to k_{off}.

For the three-state model (binding followed by a conformational change), E + I ↔ E–I ↔ E*–I, a double-exponential behavior is observed (**Supplementary Fig. 6c**). If the rates corresponding to these steps are substantially different, each step can be treated separately, and two observed rates (k^{obs}_{bind} and k^{obs}_{conf}) can be extracted from the fits of the graph of fluorescence versus time (**Supplementary Fig. 6c**,**e**).

The first step (i.e., binding) is defined by the observed binding rate k^{obs}_{bind}, and it follows the same laws as described above. In particular, the plot of k^{obs}_{bind} versus [I] will be linear, and the slope will define k_{on} and the intercept will define k_{off} (**Supplementary Fig. 6e**). The second phase corresponds to the conformational transition. The plot of k^{obs}_{conf} versus [I] is nonlinear and plateaus at the value corresponding to the sum of the k_{conf+} and k_{conf-} rate constants (**Supplementary Fig. 6e**).

The dependence of the observed rate of conformational transition on inhibitor concentration is counterintuitive, but it can be rationalized in the following way. The rate of E*–I formation is determined by the differential equation

$$\frac{d(\mathrm{E^*-I})}{dt} = k_{conf+}[\mathrm{E-I}] - k_{conf-}[\mathrm{E^*-I}]$$

meaning that it depends on the concentration of E–I. At higher inhibitor concentrations, more inhibitor will be bound, effectively increasing the transient concentration of the E–I state (**Supplementary Fig. 6d**); consequently, the observed rate of fluorescence change will increase. At very high concentrations of I, the equilibrium of the E + I ↔ E–I reaction will be heavily skewed to the right, at which point the concentration of the E–I state will no longer be [I] dependent, and the graph of k^{obs}_{conf} versus [I] will reach a plateau.

If the dissociation of I is fast, then k_{conf-} can be reliably determined in a dilution experiment, when the enzyme is first saturated with I and then diluted, causing I to dissociate. If the dissociation step (rate constant k_{off}) is much faster than k_{conf-}, then the observed fluorescence change will be monoexponential, and the rate will be limited by the k_{conf-} rate constant (remaking E–I from E*–I) (**Supplementary Fig. 6f**).

In summary, double-exponential fit of the graph of fluorescence versus time can be used to generate plots of k^{obs}_{bind} versus [I] and k^{obs}_{conf} versus [I]. The first one is linear and defines k_{on} and k_{off}, and the second one is nonlinear and defines the sum k_{conf+} + k_{conf-}. If k_{conf-} is independently determined in the dilution experiment, then both k_{conf+} and k_{conf-} can be calculated. Thereby the system is fully determined.

33. Ericsson, U.B., Hallberg, B.M., Detitta, G.T., Dekker, N. & Nordlund, P. Thermofluor-based high-throughput stability optimization of proteins for structural studies. *Anal. Biochem.* **357**, 289–298 (2006).
34. Delaglio, F. *et al.* NMRPipe: a multidimensional spectral processing system based on UNIX pipes. *J. Biomol. NMR* **6**, 277–293 (1995).
35. Vranken, W.F. *et al.* The CCPN data model for NMR spectroscopy: development of a software pipeline. *Proteins* **59**, 687–696 (2005).

doi:10.1038/nsmb.2891